LBL-17148
c.2

Lawrence Berkeley Laboratory
UNIVERSITY OF CALIFORNIA

RECEIVED
LAWRENCE
BERKELEY LABORATORY
MAR 14 1984
LIBRARY AND
DOCUMENTS SECTION

Accelerator & Fusion Research Division

Presented at the Fluids and Plasmas: Geometry and Dynamics Conference, Boulder, CO, July 17-23, 1983

HOPF BIFURCATION AND THE BEAM-PLASMA INSTABILITY

J.D. Crawford

January 1984

TWO-WEEK LOAN COPY
This is a Library Circulating Copy which may be borrowed for two weeks. For a personal retention copy, call Tech. Info. Division, Ext. 6782.

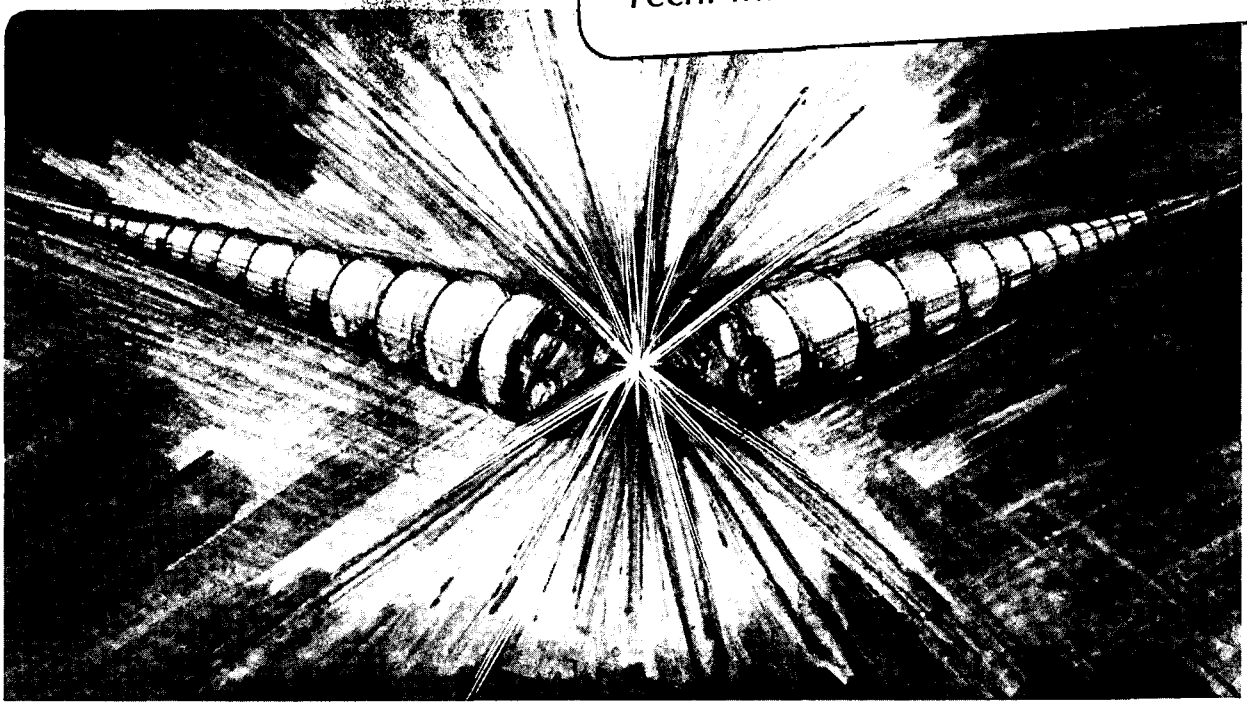

LBL-17148 c.2

Prepared for the U.S. Department of Energy under Contract DE-AC03-76SF00098

DISCLAIMER

This document was prepared as an account of work sponsored by the United States Government. While this document is believed to contain correct information, neither the United States Government nor any agency thereof, nor the Regents of the University of California, nor any of their employees, makes any warranty, express or implied, or assumes any legal responsibility for the accuracy, completeness, or usefulness of any information, apparatus, product, or process disclosed, or represents that its use would not infringe privately owned rights. Reference herein to any specific commercial product, process, or service by its trade name, trademark, manufacturer, or otherwise, does not necessarily constitute or imply its endorsement, recommendation, or favoring by the United States Government or any agency thereof, or the Regents of the University of California. The views and opinions of authors expressed herein do not necessarily state or reflect those of the United States Government or any agency thereof or the Regents of the University of California.

LBL-17148

HOPF BIFURCATION AND THE BEAM-PLASMA INSTABILITY*

John David Crawford**

Lawrence Berkeley Laboratory

and

Physics Department

University of California, Berkeley

Berkeley, California 94720

---

* This work was supported by the Director, Office of Energy Research, Office of Fusion Energy, Basic Energy Sciences Division of the U.S. Department of Energy under Contract No. DE-AC03-76SF00098.

** Current Address: Physics Dept. University of California, San Diego, La Jolla, CA 92037

ABSTRACT

For finite mode instabilities in dissipative systems, invariant manifold methods allow the bifurcation analysis to be reduced to the locally attracting center manifold. In a kinetic model of electron plasma dynamics, these methods are applied to the one mode beam-plasma instability which occurs via Hopf bifurcation. The instability results in a nonlinear oscillation, and the amplitude equation can be solved to describe the time asymptotic state.

Introduction

I shall describe results on a simple plasma model which exhibits a beam-plasma instability as a Hopf bifurcation. The analysis is geometric in that it utilizes the notion of an invariant center manifold to reduce the problem to two dimensions. Since Hopf bifurcation can be analyzed by other techniques as well[1], it is worthwhile to review those aspects of the geometric methods which are particularly valuable.

In dissipative systems, even in infinite dimensions, when an equilibrium becomes unstable due to a finite number of unstable linear modes, the nonlinear dynamics of the instability is finite dimensional, i.e. the dynamics may be described by a finite dimensional vector field. An appreciation of the stable and center manifolds associated with the equilibrium makes this fact simple and intuitive.

In addition to this conceptual virtue, the geometric point of view offers practical advantages as well. By deriving (approximately) the vector field on the center manifold, one obtains the finite dimensional dynamics which captures all the (local) qualitative behavior exhibited by the instability. Although these results are essentially perturbative and therefore only apply near the threshold for the instability, there is no requirement that a specific parameter be chosen

as the bifurcation parameter, and the relevant finite dimensional system may be derived without a priori assumptions about the form of the solutions, e.g., fixed points, periodic orbits, tori, strange attractors, etc. This is very helpful when the instability involves more than one or two dimensions[2].

Invariant Manifolds for Fixed Points

The general setting assumes an evolution equation,

$$\frac{dx}{dt} = \mathcal{L}_\mu x + N_\mu(x) \qquad x \in \mathcal{M} \tag{1}$$

defined on some phase space M. $\mathcal{L}_\mu$ is a linear operator and $N_\mu(\cdot)$ is a smooth nonlinear operator satisfying $N_\mu(0) = 0$. Both $\mathcal{L}_\mu$ and N_μ may depend on physical parameters μ. $\mathcal{M}$ may be a finite dimensional manifold, or an appropriately chosen function space for infinite dimensional problems. (The technical issues involved when proving the existence of center manifolds for partial differential equations are discussed by Holmes and Marsden[3].)

The state $x=0$ is an equilibrium and its linear stability is governed by the spectrum of $\mathcal{L}_\mu$, denoted $\sigma(\mathcal{L}_\mu)$. Emphasizing here the finite dimensional case for illustration, suppose $\sigma(\mathcal{L}_\mu)$ contains n_s eigenvalues in the left half plane, n_c eigenvalues on the imaginary axis, and n_u eigenvalues in the right half plane as shown in Figure (1a). Barring the

occurrence of degeneracy,

$$n_s + n_c + n_u = \dim M ,$$

and the associated eigenvectors span the stable subspace E^s, the center subspace E^c, and the unstable subspace E^u, respectively. These subspaces are invariant under the linearized dynamics

$$\frac{dx}{dt} = \mathcal{L}_\mu x ,$$

and determine the qualitative features of the linearized flow as shown in Figure (1b).

When the nonlinear effects represented by $N_\mu(x)$ are restored, the dynamics of linear eigenvectors are coupled, and the linear subspaces E^s, E^c, and E^u are no longer invariant. There are, however, nonlinear analogues of the linear subspaces. Intuitively, the nonlinear effects distort the solutions of the linear eigenspaces so that the flat linear eigenspaces are "warped" into curved surfaces or manifolds. These manifolds organize the dynamics of the nonlinear problem just as the linear eigenspaces serve to structure the linear dynamics.

Thus associated with the linear subspaces are the local stable, center, and unstable minifolds, denoted W^s, W^c and W^u, respectively (see Figure (2a))[4]. Each local manifold

contains $x=0$ and is tangent at $x=0$ to the appropriate linear subspace. Thus each manifold has the same dimension as its associated linear subspace. Furthermore, each local manifold is invariant with respect to the full nonlinear dynamics: if an initial condition $x(0)$ belongs to W^s, W^c, or W^u then for $0 < t < T$ the solution $x(t)$ to (1) lies within the manifold containing $x(0)$.

The dynamics of solution curves in W^s or W^u is trivial, at least near $x=0$. As $t \to \infty$ solution curves in W^s approach $x=0$, and as $t \to -\infty$ solutions in W^u approach $x=0$; in both cases the asymptotic rate of approach is exponential since the linearized dynamics dominates. No such simple characterization is possible for the dynamics in W^c; at $x=0$ the linear stability is neutral and nonlinear effects remain essential. When the dimension of W^c is greater than two, the center manifold dynamics may encompass all the complex dynamics studied in dynamical systems theory: aperiodic motion, chaotic recurrence, Smale horseshoes, strange attractors, etc.

Hopf Bifurcation

Suppose for $\mu < 0$ the equilibrium $x=0$ is stable ($n_u = n_c = 0$, $n_s = \dim M$) but as μ increases through $\mu = 0$ a simple conjugate pair of eigenvalues $\lambda, \bar{\lambda}$ crosses into the right half plane, then we typically have a Hopf

bifurcation, see Figure (2b) for the spectrum at $\mu = 0$. Denote by ψ and $\bar{\psi}$ the eigenvectors of this pair, so

$$\mathcal{L}_\mu \psi = \lambda \psi$$
$$\mathcal{L}_\mu \bar{\psi} = \bar{\lambda} \bar{\psi}.$$

For the application considered here, at bifurcation a stable periodic orbit emerges from the equilibrium; physically one observes a time independent state yield to a single frequency oscillation. In Couette flow a beautiful example of this phenomenon is the transition from the Taylor vortex state to the flow with a rotating wave[5].

For the spectrum of Figure (2b), the fixed point $x=0$ will have a two dimensional center manifold and a stable manifold of dimension $(\dim M)-2$, see Figure (3a). As μ increases above $\mu = 0$, the center manifold is replaced by a two dimensional unstable manifold (assuming no other spectral elements cross the axis). Let W_μ denote this one parameter family of two dimensional invariant manifolds, i.e. $W_{\mu=0} = W^c$ and $W_{\mu>0} = W^u$; for μ near 0. W_μ is <u>locally attracting</u> because of the strong contraction provided by W^s in the "transverse" directions[6]. Specifically, there is a neighborhood of $x=0$ such that all solutions remaining in that neighborhood as $t \to \infty$ will approach W_μ. Thus the flow on W_μ, which is given by a two dimensional vector field, describes the time asymptotic motion. This reduction in

dimension as $t \to \infty$ greatly simplifies the problem, and suggests the following strategy: "project out" the two dimensional vector field which describes the flow on W_μ, then analyze that flow to understand the asymptotic development of the instability.

The Model

Consider a one dimensional plasma of finite length L and periodic boundary conditions. For the study of high frequency electrostatic waves, the ion dynamics may be neglected, and the electron distribution function $F(x,v,t)$ evolves according to

$$\begin{aligned} \frac{\partial F}{\partial t} + v\frac{\partial F}{\partial x} + \frac{e}{m}\frac{\partial \phi}{\partial x}\frac{\partial F}{\partial v} &= C(F) \\ -\frac{\partial^2 \phi}{\partial x^2} &= 4\pi e n_0 \left[1 - \int_{-\infty}^{\infty} dv\, F(x,v,t)\right] \end{aligned} \tag{2}$$

where (x,v) are the electron position and velocity, $n_0 = N/L$ is the mean density, and $-e/m$ is the electron charge/mass ratio[7]. Normalize F such that

$$n_0 \int_{-\infty}^{\infty} dv\, F(x,v,t) = n(x,t) = \text{density of electrons}$$

and

$$\int_0^L dx\; n(x,t) = N.$$

For the collision model $C(F)$ take the Krook operator

$$C(F) = \nu_c \left(F_{eq} - F \right)$$

where $\nu_c > 0$, and

$$F_{eq}(x,v) = \frac{n(x,t)}{n_o} g_{eq}(v).$$

This collision model conserves the particle density since

$$\int_{-\infty}^{\infty} dv \; C(F) = 0$$

but not energy or momentum[8].

For an initially homogeneous, nonequilibrium state, $F_1(x,v,t=0) = F_0(v) \neq g_{eq}(v)$, the self-consistent electric field is zero,

$$\left. \frac{\partial \phi_1}{\partial x} \right|_{t=0} = 0,$$

and the dynamics reduces to

$$\frac{\partial F_1}{\partial t} = C(F_1)$$

with solution

$$F_1(x,v,t) = g_{eq}(v) + \left(F_0(v) - g_{eq}(v) \right) e^{-\nu_c t}$$

Since $C(F)$ conserves $n(x,t)$, no spatial dependence develops so

$$\frac{\partial \phi_1}{\partial x} = 0 \qquad \text{for} \quad t \geq 0.$$

If, however, the initial condition is perturbed so that

$$F_2(x,v,t=0) = F_0(v) + f(x,v,t=0) \ ,$$

then, depending on the shape of F_0, the resulting electric fields may drive the growth of unstable waves. To study this one writes an equation for $\partial_t f = \partial_t F_2 - \partial_t F_1$,

$$\frac{\partial f}{\partial t} + v\frac{\partial f}{\partial x} + \frac{e}{m}\frac{\partial \phi_f}{\partial x}\frac{\partial (F_0+f)}{\partial v} = -\nu_c\left[f - g_{eq}\int_{-\infty}^{\infty} dv' f(x,v',t)\right]$$

$$\frac{\partial^2 \phi_f}{\partial x^2} = 4\pi e n_0 \int_{-\infty}^{\infty} dv\, f(x,v,t) \tag{3}$$

where the approximation $\frac{\partial F_1}{\partial v} \simeq \frac{\partial F_0}{\partial v}$ has been used in the nonlinear term to obtain an autonomous description of $f(x,v,t)$[7]. By introducing the Fourier expansions,

$$f(x,v,t) = \sum_k f_k(v,t)\, e^{ikx}$$

$$\phi_f(x,t) = \sum_k \phi_k(t)\, e^{ikx}$$

where $\Delta k = 2\pi/L$, and eliminating ϕ_f, then (3) yields an evolution equation for f,

$$\frac{\partial f}{\partial t} = \mathcal{L} f + N(f). \tag{4}$$

The linear operator in (4) is defined by

$$\mathcal{L} f = \sum_k e^{ikx}(L_k f_k)(v)$$

where

$$L_0 f_0 = -\nu_c f_0$$

$$L_k f_k = -\left[(ikv+\nu_c) f_k + ik\eta_k \int_{-\infty}^{\infty} dv' f_k(x,v',t)\right] \qquad k \neq 0$$

with

$$\eta_k(v) = -\left(\frac{\omega_e}{k}\right)^2 \frac{\partial F_0}{\partial v} + \left(\frac{i\nu_c}{k}\right) g_{eq}(v)$$

and the nonlinear operator in (4) is

$$N(f) = \sum_{\ell} e^{i\ell x} \sum_{k\neq 0} \frac{i\omega_e^2}{k} \frac{\partial f_{\ell-k}}{\partial v} \int_{-\infty}^{\infty} dv' f_k(x,v',t).$$

Here $\omega_e^2 = 4\pi e^2 n_0/m$ is the plasma frequency. In (4), the point $f=0$ is a stationary solution; physically, it corresponds to the distribution function $F_0(v)$.

Linear Stability

The calculation of $\sigma(\mathcal{L})$ follows Case closely and will be described elsewhere[7,9]. The results are illustrated in Figure (4a). There is a line of continuous spectrum at $\mathrm{Re}\,\lambda = -\nu_c$ with eigenfunctions which are distributions. There may also be discrete eigenvalues; these are determined by the roots of the dispersion function,

$$\Lambda_k(z) = 1 + \int_{-\infty}^{\infty} \frac{\eta_k(v)\,dv}{v-z}, \quad z \in \mathbb{C}. \tag{5}$$

If $\Lambda_k(z) = 0$, then $\Lambda_{-k}(\bar{z}_0)=0$ and $\sigma(\mathcal{L})$ contains a conjugate eigenvalue pair

$$\lambda_1 = -\nu_c - ikz_0 = \bar{\lambda}_2$$

with eigenfunctions

$$\psi = e^{ikx}\left(\frac{-\eta_k}{v-z_0}\right)$$

$$\bar{\psi} = e^{-ikx}\left(\frac{-\bar{\eta}_k}{v-\bar{z}_0}\right)$$

satisfying

$$\mathcal{L}\psi = \lambda_1\psi$$
$$\mathcal{L}\bar{\psi} = \bar{\lambda}_1\bar{\psi}\,.$$

In the limit $\nu_c \to 0$, $\Lambda_k(z)$ is even in k, and the eigenvalues of $\mathcal{L}$ form quadruplets as shown in Figure (4b). The fundamental reason for this is the Hamiltonian structure of the Vlasov-Poisson system[10].

Following Case, define the inner product,

$$\langle\phi,\psi\rangle \equiv \int_0^L dx \int_{-\infty}^{\infty} \bar{\phi}(x,v)\,\psi(x,v),$$

and the adjoint operator $\mathcal{L}^+$,

$$\langle\phi,\mathcal{L}\psi\rangle = \langle\mathcal{L}^+\phi,\psi\rangle$$

The eigenfunctions of $\mathcal{L}^+$ and $\mathcal{L}$ satisfy biorthogonality relations analogous to those found by Case for the $\nu_c = 0$

problem[9]. In particular, the adjoint eigenvectors for λ_1 and $\bar{\lambda}_1$,

$$\mathcal{L}^{+}\tilde{\psi} = \bar{\lambda}_1 \tilde{\psi}$$
$$\mathcal{L}^{+}\tilde{\bar{\psi}} = \lambda_1 \tilde{\bar{\psi}},$$

satisfy $\langle \tilde{\psi}, \psi \rangle = \langle \tilde{\bar{\psi}}, \bar{\psi} \rangle = 1$, and are orthogonal to all other eigenvectors of $\mathcal{L}$.

When the initial state $F_0(v)$ is sufficiently close to $g_{eq}(v)$, then $\sigma(\mathcal{L})$ is contained within the left half plane as shown in Figure (4a)[7]. If $F_0(v)$ is distorted, for example by adding a component of electrons at high velocity ("the beam"), then it is possible for a complex conjugate pair of eigenvalues $\lambda_1, \bar{\lambda}_1$ to cross the imaginary axis signaling the onset of of growing electrostatic waves. For suitably chosen length L, the first unstable mode corresponds to the minimum wave number $k = 2\pi/L$. The remainder of this discussion concerns the analysis of this one mode instability.

Center Manifold Dynamics

As the procedure for calculating the center manifold vector field is fully discussed in recent texts, I will simply outline the calculation[4,6]. By defining the complex amplitude

$$A(t) = \langle \tilde{\psi}, f \rangle,$$

the perturbation may be decomposed as,

$$f(x,v,t) = A(t)\psi(x,v) + \overline{A(t)}\,\bar{\psi}(x,v) + S(x,v,t) \tag{6}$$

where $\langle \tilde{\psi}, S \rangle = \langle \tilde{\bar{\psi}}, S \rangle = 0$. The evolution equation (4) is then rewritten,

$$\begin{aligned} \dot{A}(t) &= \lambda_1 A + \langle \tilde{\psi}, N(f) \rangle \\ \frac{\partial S}{\partial t} &= \mathcal{L} S + N(f) - \langle \tilde{\psi}, N(f) \rangle - \overline{\langle \tilde{\psi}, N(f) \rangle}. \end{aligned} \tag{7}$$

To restrict (7) to W_μ, the two dimensional invariant manifold associated with the bifurcation (μ now denotes the physical parameters in the distribution function), introduce local coordinates on W_μ near the fixed point, see Figure (3b). The function $h(A,\bar{A})$ measures the deviation of W_μ from the $(\psi,\bar{\psi})$-plane. An element of W_μ near the fixed point therefore has the form,

$$f^c(x,v,t) = A(t)\psi(x,v) + \bar{A}(t)\bar{\psi}(x,v) + h(x,v,A(t),\bar{A}(t)). \tag{8}$$

Inserting (8) into (7) yields

$$\dot{A} = \lambda_1 A + \langle \tilde{\psi}, N(f^c) \rangle \tag{9}$$

which is an autonomous equation for $A(t)$; this determines the evolution of f^c in (8).

To make practical use of (9) requires an explicit representation for $h(A,\bar{A})$. An equation for h follows from the observation that for solutions f^c in (8) there are two ways to compute the rate of change of $S^c(x,v,t) = h(x,v,A,\bar{A})$. From (7) directly,

$$\frac{\partial S^c}{\partial t} = \mathcal{L} S^c + N(f^c) - \langle \tilde{\Psi}, N(f^c) \rangle - \overline{\langle \tilde{\Psi}, N(f^c) \rangle} \tag{10}$$

or from (8)

$$\frac{\partial S^c}{\partial t} = \left[\frac{\partial h}{\partial A} \dot{A} + \frac{\partial h}{\partial \bar{A}} \dot{\bar{A}} \right] \Bigg|_{f=f^c} \tag{11}$$

Equating the right hand sides of (10) and (11) provides the desired equation for h which is then solved using a power series in $A,\bar{A}$. To lowest nontrivial order, this power series has the form

$$h(x,v,A,\bar{A}) = h^{(1)}(x,v) A^2 + h^{(2)}(x,v) |A|^2 + \overline{h^{(1)}(x,v)} \bar{A}^2 + \cdots$$

where

$$h^{(1)}(x,v) = e^{i2kx} h^{(1)}_{2k}(v)$$

$$h^{(2)}(x,v) = h^{(2)}_0(v) .$$

$h_{2k}^{(1)}(v)$ and $h_0^{(2)}(v)$ are explicitly computable functions of velocity[7]. Knowing $h(A,\bar{A})$ to quadratic order in A, determines (9) to cubic order,

$$\dot{A} = \lambda_1 A + \beta |A|^2 A + \mathcal{O}(A^4) \tag{12}$$

where

$$\beta = \frac{i\omega_e^2}{k} \left\langle \tilde{\Psi}, e^{ikx} \left[\frac{\partial}{\partial v}\left(h_0^{(2)} - h_{2k}^{(1)}\right) + \frac{1}{2} H \frac{\partial}{\partial v} \Psi_{z_0} \right] \right\rangle \tag{13}$$

$$H = \int_{-\infty}^{\infty} dv \, h_{2k}^{(1)}(v)$$

$$\Psi_{z_0} = \left(\frac{-\eta_k}{v - z_0} \right).$$

In polar variables, $A = \rho(t) e^{i\theta(t)}$, the amplitude equation (12) becomes,

$$\dot{\rho} = (\mathrm{Re}\,\lambda_1)\rho + (\mathrm{Re}\,\beta)\rho^3 + \cdots \tag{14}$$

$$\dot{\theta} = \mathrm{Im}\,\lambda_1 + (\mathrm{Im}\,\beta)\rho^2 + \cdots$$

When the conjugate pair associated with the instability has just entered the right half plane, then $0 < \mathrm{Re}\,\lambda_1 << 1$, and the instability will saturate at small amplitude, i.e., $\dot{\rho} = 0$ for $0 < \rho << 1$, only if $\mathrm{Re}\,\beta < 0$. The saturated amplitude is

$$\rho_s^2 \sim \left(\frac{-\mathrm{Re}\,\lambda_1}{\mathrm{Re}\,\beta}\right).$$

<u>Results for Lorentzian Beams and Plasmas</u>

For simplicity let the equilibrium distribution be

$$g_{eq}(v) = \frac{1}{\pi}\left(\frac{\alpha}{v^2+\alpha^2}\right),$$

and take as the initial distribution (corresponding to f=0)

$$n_0 F_0(v) = n_p F_p(v) + n_b F_b(v)$$

$$= \frac{1}{\pi}\left[\frac{\alpha n_p}{v^2+\alpha^2} + \frac{\delta n_b}{(v-u)^2+\delta^2}\right]$$

where $n_p F_p$ is the plasma distribution, $n_b F_b$ is the beam distribution, α is the plasma temperature, δ is the beam temperature, and u is the beam velocity. Consider the case of a low density, cool beam; specifically choose

$$\varepsilon \equiv \nu_c/\omega_e = 0.001$$

$$\delta/\alpha = 0.5$$

$$n_b/n_0 = 0.05$$

$$n_p/n_0 = 0.95\,.$$

The roots of the dispersion function vary with the wave number k and the beam velocity u. Since $\lambda_1 = -\nu_c - ikz_0$, points in the (k,u)-plane for which $\mathrm{Im}\, z_0 = \nu_c/k$ correspond to criticality. This surface is the solid curve in Figure (5a). For $k = 0.17$ the real parts of the dispersion roots appear in Figure (5b) as a function of u. The condition for instability

$$\mathrm{Im}\, z_0 > \nu_c/k \tag{15}$$

is fulfilled along the indicated branch of the dispersion function.

The cubic coefficient β has a negative real part along the bifurcation surface in Figure (5a), and also along the vertical line marking $k = 0.17$[7]. We may, therefore, evaluate the approximate expression for the saturated distribution,

$$F_2(x,v,t) \approx F_0(v) + A_s(t)\psi(x,v) + \bar{A}_s(t)\psi(x,v) + A_s^2 h_{2k}^{(1)}(v)\, e^{i2kx} + |A_s|^2 h_0^{(2)}(v) + \bar{A}_s^2 \overline{h_{2k}^{(1)}}\, e^{-i2kx} + \cdots$$

where

$$A_s(t) = \rho_s\, e^{i\theta(t)}$$

$$\theta(t) = \left[\mathrm{Im}\,\lambda_1 + (\mathrm{Im}\,\beta)\rho_s^2 + \cdots\right]t + \theta(0).$$

Of greatest interest is the spatially homogeneous component,

$$F_0(v) + \rho_s^2 h_0^{(2)}(v) + \cdots \tag{16}$$

as seen from the frame of reference moving at the phase velocity of the wave v_w. The coordinates of this frame are (x', v'),

$$x' = x - v_w t$$

$$v' = v - v_w$$

$$v_w = \frac{-1}{k}\frac{d\theta}{dt} .$$

Figure (6a) shows the unperturbed distribution corresponding to point A in Figure (5a) where the growth rate γ of the instability is relatively small. Figure (6b) shows the shape of the lowest order correction to the unperturbed distribution. The basic effect is to slow down the resonant particles which move at $v' \approx 0$. The saturated component of (16) for point A appears in Figure (7).

At point B in Figure (5a) the linear growth rate is approximately two orders of magnitude larger. The shape of $h_0^{(2)}$ in Figure (8a) now reveals some broadening of the plasma distribution as well as a strong acceleration of the resonant particles. Figure (8b) shows the unperturbed and saturated distributions.

Final Remarks

1) Although I have concentrated on the one mode instability, this model exhibits a codimension two double Hopf bifurcation. The dotted curve in Figure (5a) is the bifurcation surface for the mode at $2k$. For the parameters at which the two bifurcation surfaces cross, there are two conjugate pairs of eigenvalues on the imaginary axis simultaneously. Here the dynamics of the instability is four dimensional and one expects much more complicated phenomena[4].

2) When $\nu_c \to 0$, the expansion coefficients $h^{(1)}$ and $h^{(2)}$ in the power series for h become singular at $v = v_w$. The presence of these singular resonance denominators is intimately related to the Hamiltonian structure of the collisionless model, and to the fact that at criticality the eigenvalues are now embedded in the continuum, see Figure (4b). Whether the collisionless instability has finite dimensional dynamics is not known. Previous treatments have assumed that the continuum does not affect the dynamics[11]. In light of the delicacy of Hamiltonian bifurcations, this assumption needs specific justification. An analysis of the collisionless instability which will extend the geometric approach discussed here, and explicitly acknowledge the Hamiltonian structure of Vlasov-Poisson dynamics is underway.

References

1. G. Iooss and D.D. Joseph, Elementary Stability and Bifurcation Theory, Springer-Verlag, Berlin, 1980.
2. J. Guckenheimer, Multiple bifurcation problems of codimension two, Siam J. Math. Analysis, in press, 1984.
3. P.J. Holmes and J. Marsden, Bifurcation to divergence and flutter in flow-induced oscillations: an infinite dimensional analysis, Automatica, 14 (1978), 367.
4. J. Guckenheimer and P. Holmes, Nonlinear Oscillations, Dynamical Systems and Bifurcations of Vector Fields, Springer Applied Math. Sciences, 43 (1983).
5. H. Swinney, these proceedings; R.C. DiPrima and H. Swinney, Instabilities and Transition in Flow Between Concentric Rotating Cylinders, in Hydrodynamic Instabilities and the Transition to Turbulence, Topics in Applied Physics, 45 (1981), Springer-Verlag, Berlin; also D. Rand, Dynamics and Symmetry: Predictions for Modulated Waves in Rotating Fluids, Arch. Rational Mech. Anal., 79 (1982), 1.
6. The one parameter family of manifolds W_μ is the three dimensional center manifold of the "suspended" system. See Ref. 4 and B.D. Hassard, N.D. Kazarinoff, and Y-H. Wan, Theory and Applications of Hopf Bifurcation, London Math. Society Lec. Notes, 41, Cambridge Univ. Press, Cambridge (1981).

7. B. Small, J.D. Crawford, and H. Abarbanel, Effects of Collisions on Longitudinal Plasma Oscillations, preprint (1983); J.D. Crawford, Hopf Bifurcation and Plasma Instabilities, Ph.D. Thesis, University of California, Berkeley (1983); J.D. Crawford and H. Abarbanel, Hopf Bifurcation in Plasma Kinetic Theory, preprint (1983).

8. P.L. Bhatnager, E.P. Gross, and M. Krook, A Model for Collision Processes in Gases. I. Small Amplitude Processes in Charged and Neutral One-Component Systems, Phys. Rev., 94 (1954), 511; and N.A. Krall and A.W. Trivelpiece, Principles of Plasma Physics, McGraw Hill, New York (1973).

9. K. Case, Plasma Oscillations, Ann. Phys., 7 (1959), 349.

10. R. Abraham and J. Marsden, Foundations of Mechanics, Addison-Wesley, Reading, Mass. (1978); P. Morrison, The Maxwell-Vlasov equations as a continuous Hamiltonian System, Phys. Lett., 80A (1980), 383; J. Marsden and A. Weinstein, The Hamiltonian Structure of the Maxwell-Vlasov equations, Physica, 4D (1982), 394.

11. A. Simon and M. Rosenbluth, Single-mode saturation of the bump-on-tail instability: immobile ions, Phys. Fluids, 19 (1976), 1567.

FIGURE CAPTIONS

Figure 1. (a) A typical spectrum for $\mathcal{L}_\mu$ consisting of real and conjugate pairs of eigenvalues. In infinite dimensional problems, $\mathcal{L}_\mu$ may also have continuous spectrum.

(b) The linear invariant subspaces E^s, E^c, and E^u determine the structure of the linearized flow.

Figure 2. (a) The invariant manifolds W^s, W^c, and W^u are the nonlinear analogues of the linear subspaces.

(b) At criticality for a nondegenerate Hopf bifurcation, the spectrum of $\mathcal{L}_\mu$ has a simple conjugate pair of eigenvalues on the imaginary axis.

Figure 3. (a) The center manifold W^c for nondegenerate Hopf bifurcation is two dimensional.

(b) Near the fixed point, the invariant manifold W_μ may be described as the graph of a function $h(A,\bar{A})$.

Figure 4. (a) Typical spectrum of the linear operator in (4) for $\nu_c > 0$. The continuum is always present. The roots of the dispersion function determine the discrete eigenvalues.

(b) For $\nu_c = 0$, $\sigma(\mathcal{L})$ reflects the Hamiltonian structure of the dynamics. At criticality, the eigenvalue quadruplet collapses to a degenerate conjugate pair embedded in the continuum.

Figure 5. (a) Bifurcation surface for a cool, low density beam (solid line). Also shown is the bifurcation surface for $2k$ (dotted line); their intersection marks a double Hopf bifurcation. Points A and B for $k = 0.17$ are the selected points of low and high growth rate.

(b) The four roots of the dispersion function for $k = 0.17$. The real part of the frequency, $\omega = \mathrm{Re}\, k z_0$, is plotted against the drift frequency ku in units of ω_e. Only on the indicated branch is condition (15) satisfied.

Figure 6. (a) Initial velocity distribution at point A as seen in the wave frame.

(b) The lowest order correction to the spatially homogeneous component of the distribution function. Shown for point A.

Figure 7. For point A, the homogeneous component of the saturated distribution function showing the effect of the lowest order correction. $\gamma = \mathrm{Re}\, \lambda$ is the linear growth rate.

Figure 8. (a) For point B, the lowest order correction to the spatially homogeneous component of the distribution function.

(b) For point B, the initial velocity distribution (dotted line) and the homogeneous component of the saturated distribution (solid line) showing the effect of the lowest order correction.

ACKNOWLEDGEMENTS

I am grateful to H. Abarbanel, A. Kaufman, and J. Marsden for their advice and support.

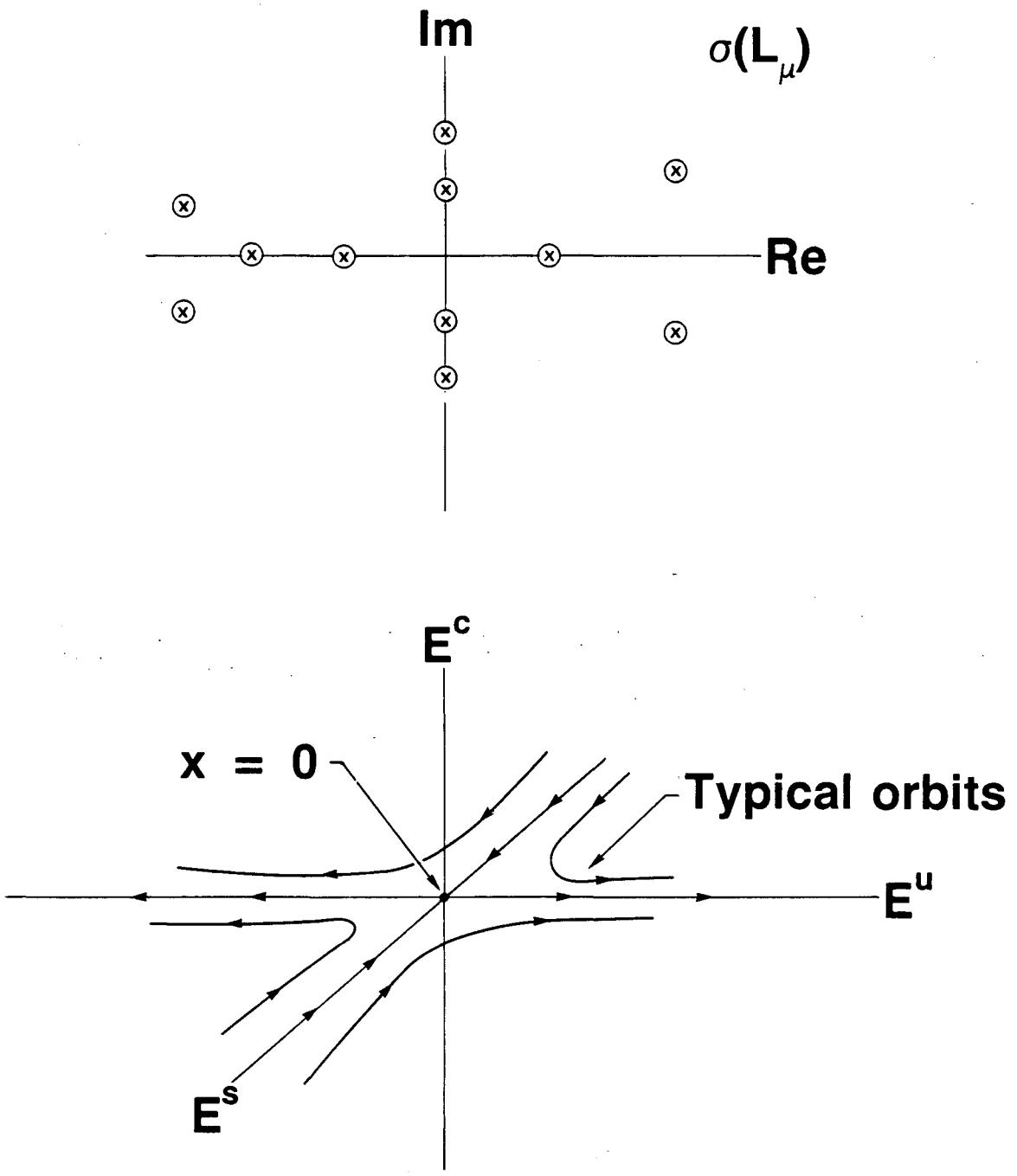

XBL 838-3011

Figure 1

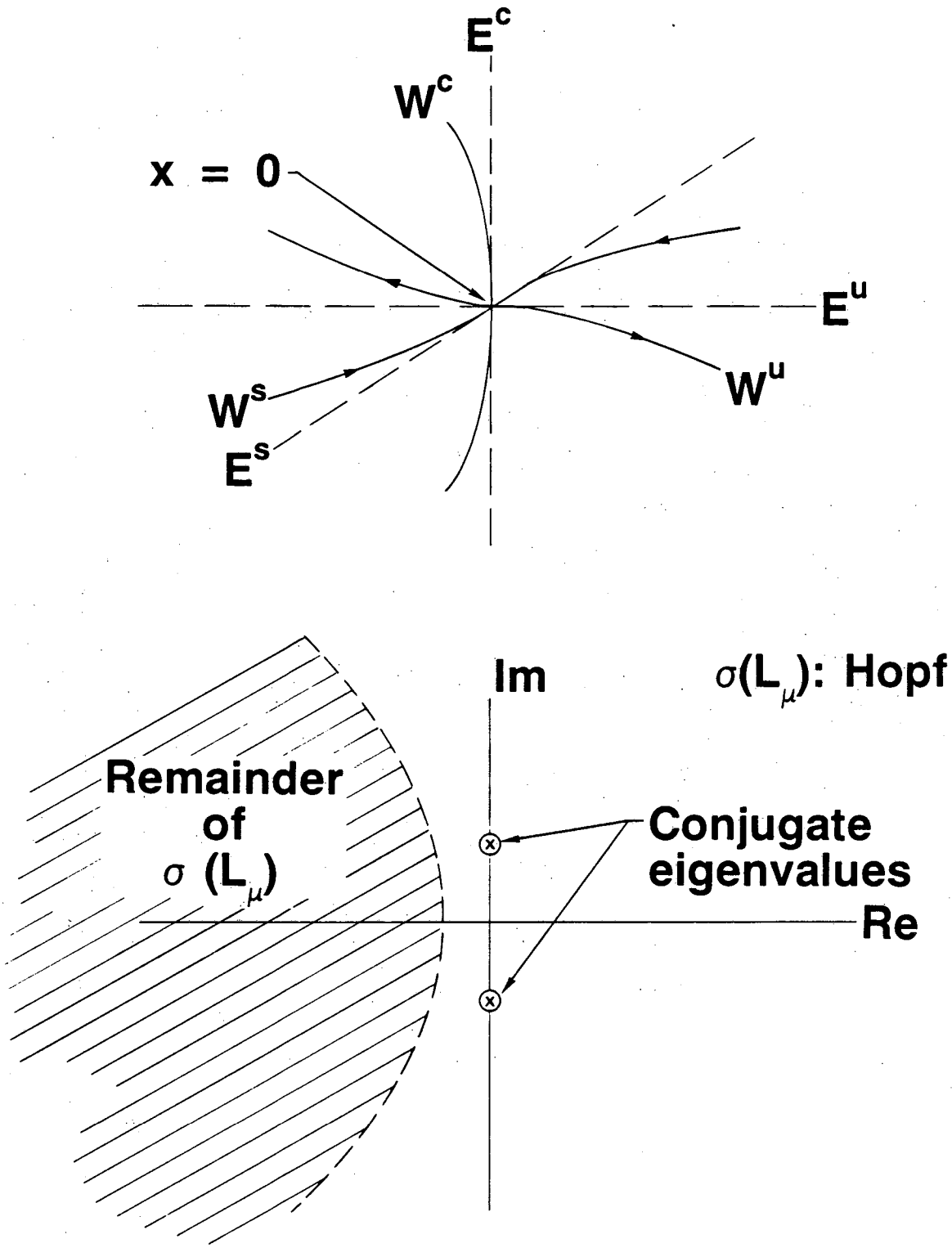

XBL 838-11194

Figure 2

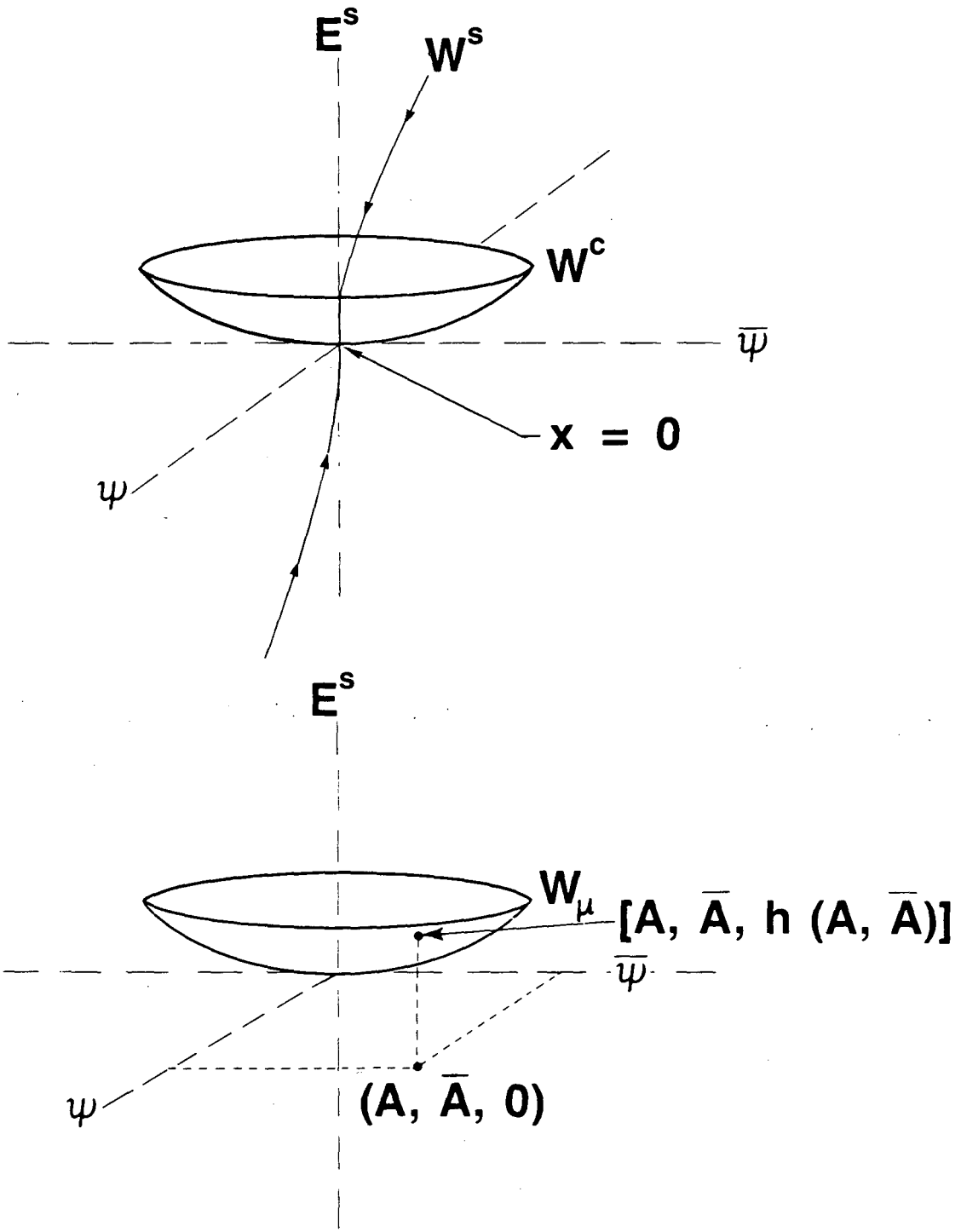

XBL 838-3005 A

Figure 3

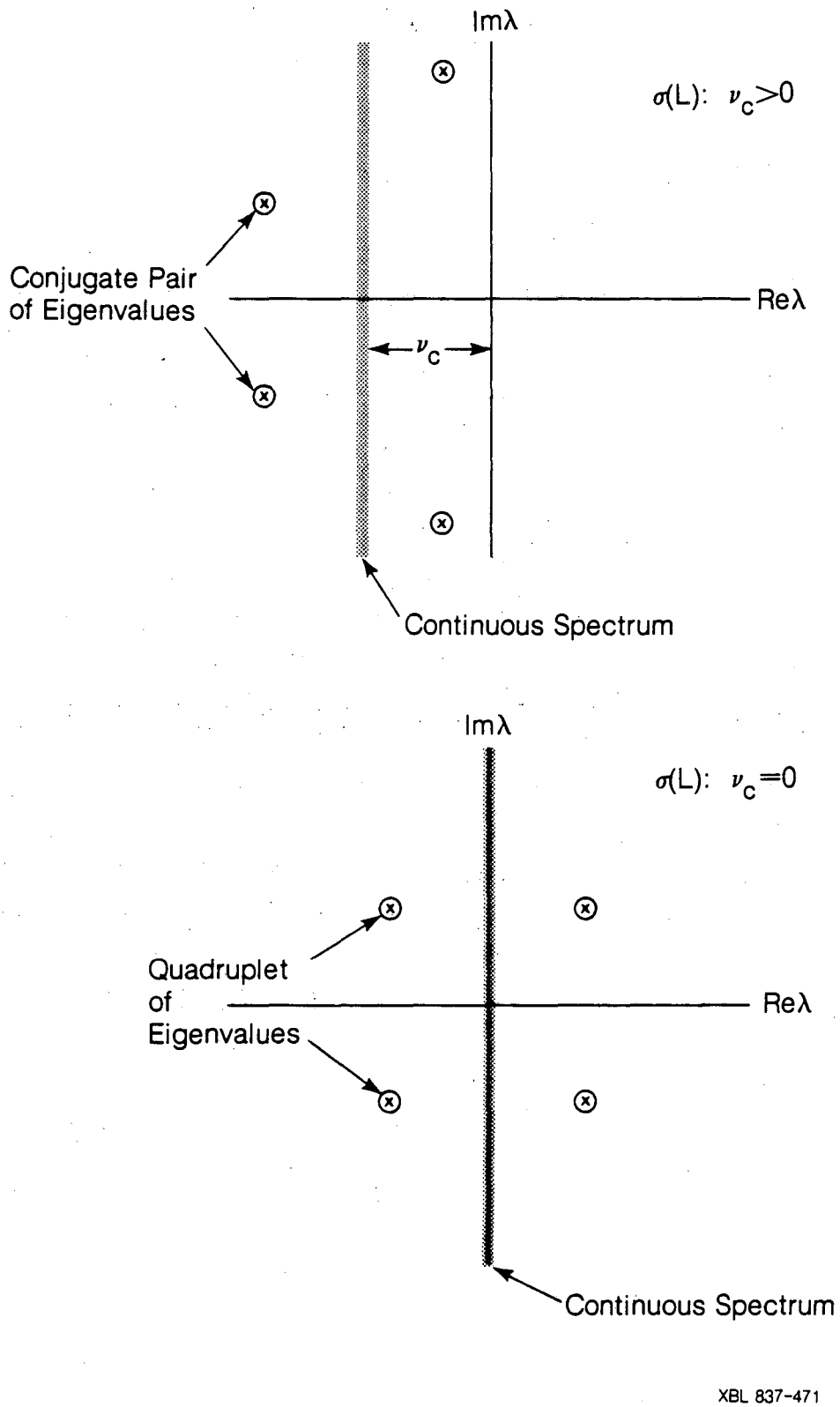
Imλ
σ(L): $\nu_c>0$
Conjugate Pair
of Eigenvalues
Reλ
ν_c
Continuous Spectrum
Imλ
σ(L): $\nu_c=0$
Quadruplet
of
Eigenvalues
Reλ
Continuous Spectrum
XBL 837-471

Figure 4

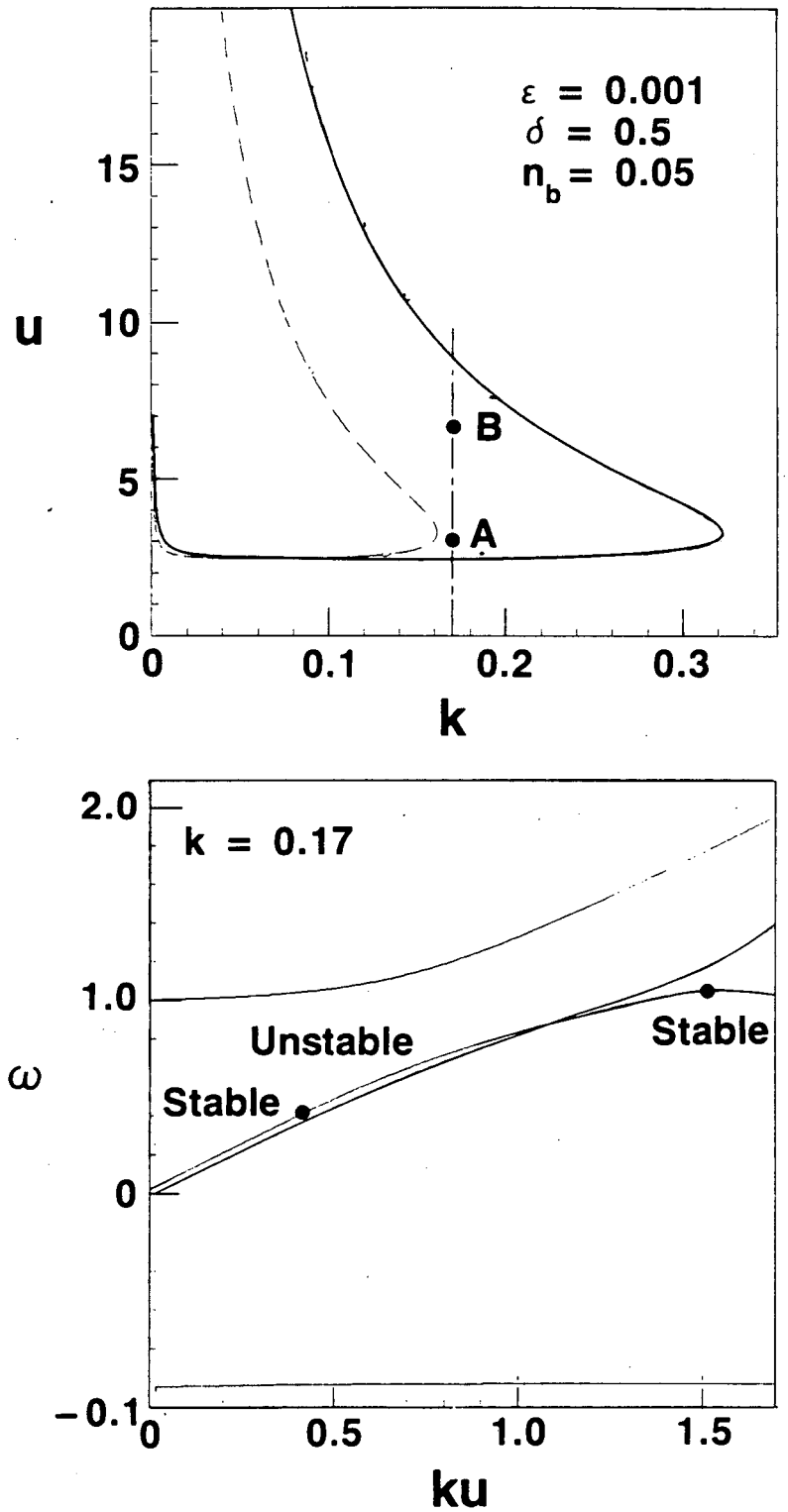

XBL 838-3007

Figure 5

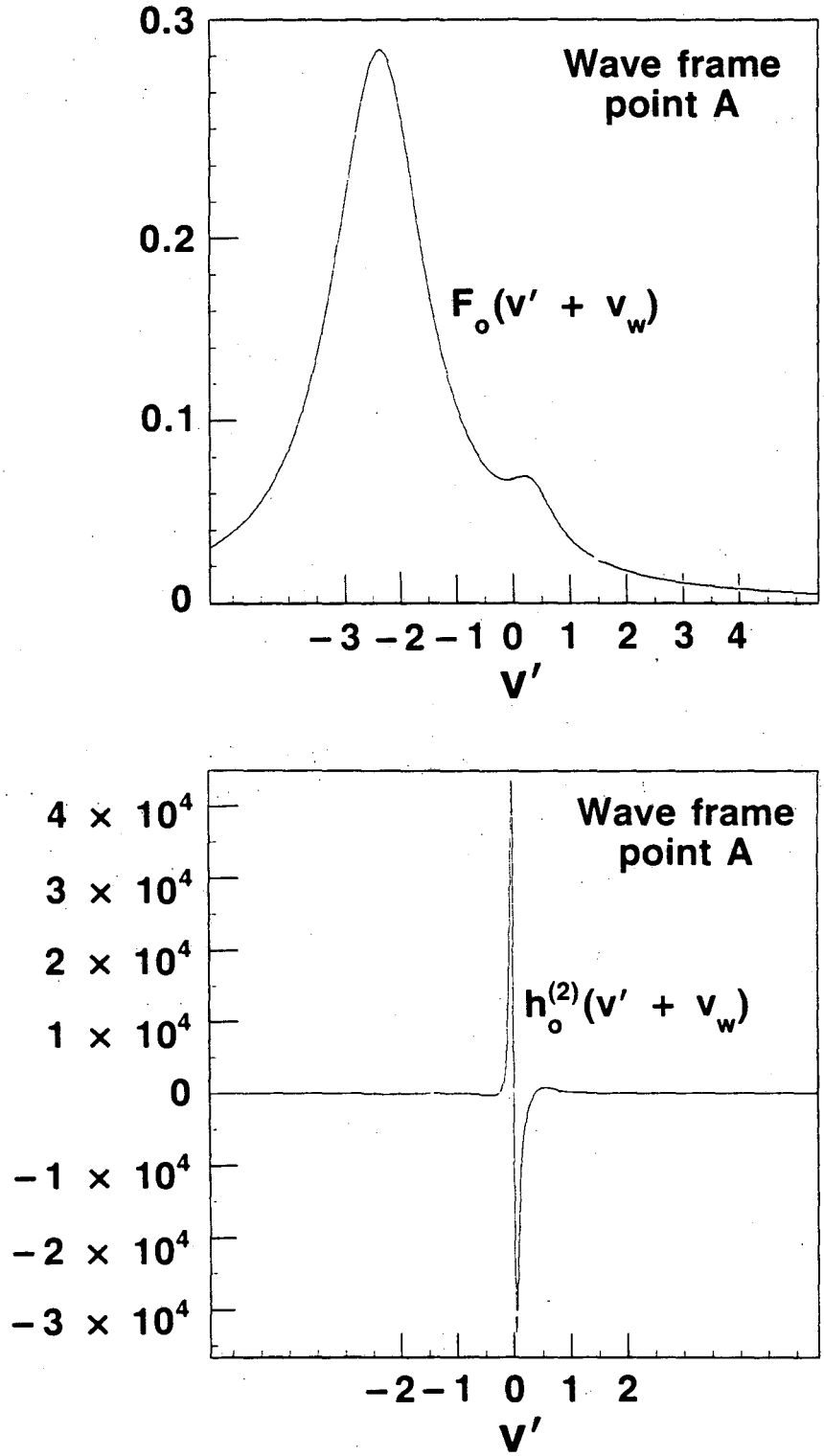
0.3
0.2
0.1
0
Wave frame
point A
$F_o(v' + v_w)$
−3 −2 −1 0 1 2 3 4
v′
4 × 10⁴
3 × 10⁴
2 × 10⁴
1 × 10⁴
0
−1 × 10⁴
−2 × 10⁴
−3 × 10⁴
Wave frame
point A
$h_o^{(2)}(v' + v_w)$
−2 −1 0 1 2
v′
XBL 838-2977

Figure 6

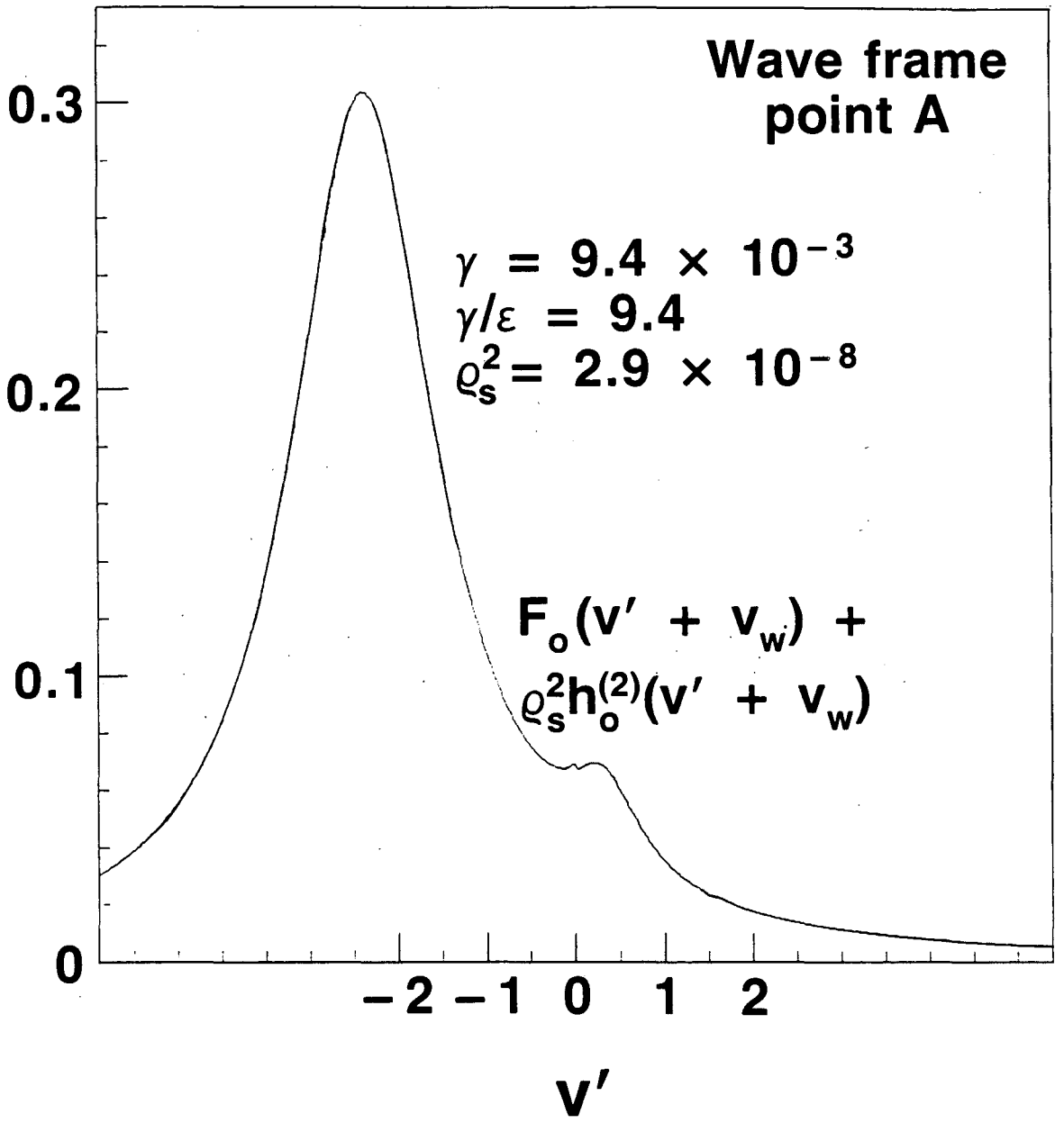

XBL 838-2974

Figure 8

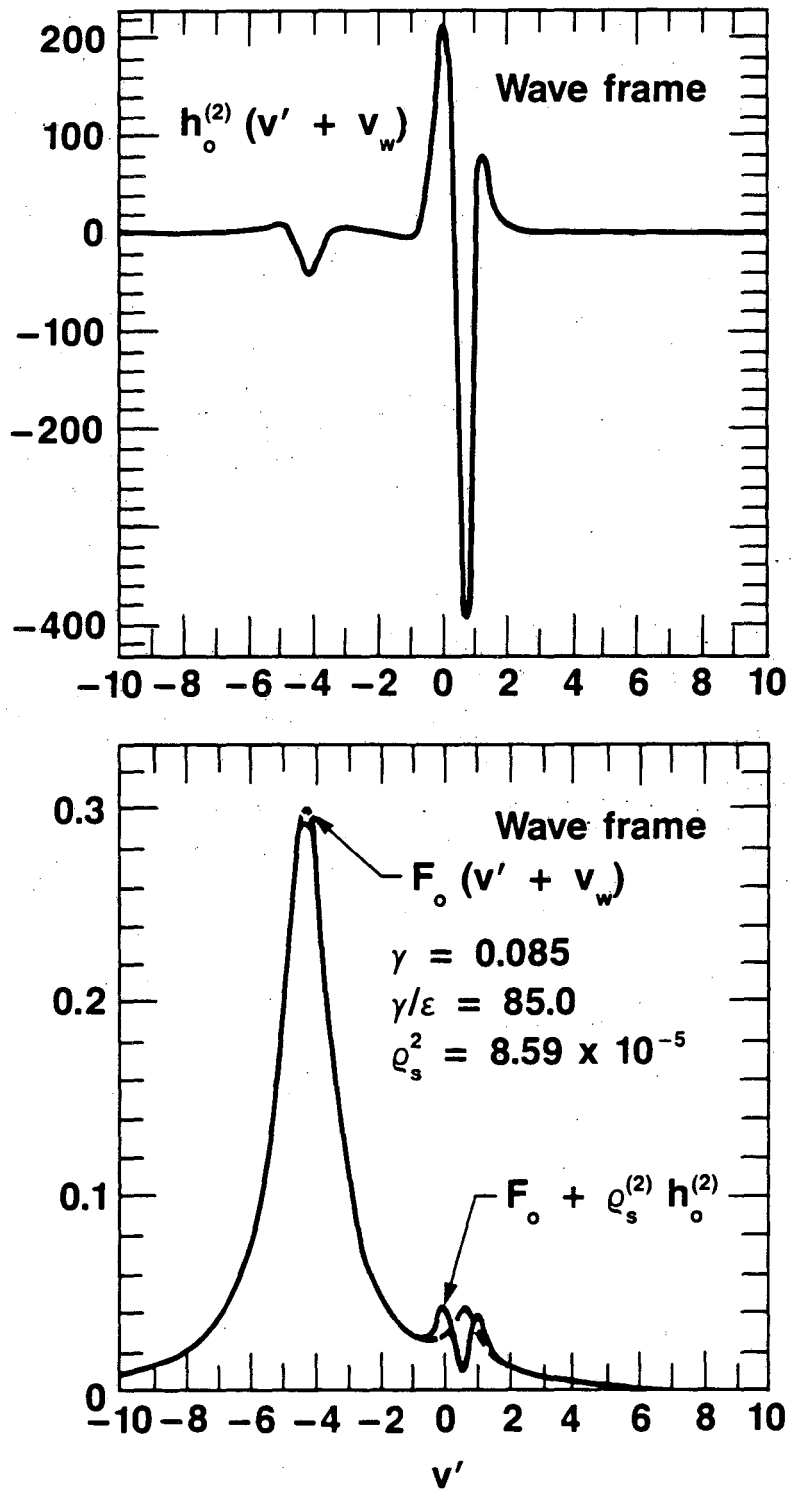

XBL 8310-12143

Figure 9

This report was done with support from the Department of Energy. Any conclusions or opinions expressed in this report represent solely those of the author(s) and not necessarily those of The Regents of the University of California, the Lawrence Berkeley Laboratory or the Department of Energy.

Reference to a company or product name does not imply approval or recommendation of the product by the University of California or the U.S. Department of Energy to the exclusion of others that may be suitable.

TECHNICAL INFORMATION DEPARTMENT
LAWRENCE BERKELEY LABORATORY
UNIVERSITY OF CALIFORNIA
BERKELEY, CALIFORNIA 94720